

# Energy decomposition analysis of metal silicide nanowires from first principles

N. Gonzalez Szwacki<sup>1,2</sup> and Boris I. Yakobson<sup>1,\*</sup>

<sup>1</sup>*Department of Mechanical Engineering & Materials Science and Department of Chemistry, Rice University, Houston, Texas 77251, USA*

<sup>2</sup>*Institute of Physics PAS, 02-668 Warsaw, Poland*

(Received 31 August 2006; published 8 January 2007)

We investigate the structure, stability, and electronic properties of yttrium silicide nanowires with AIB<sub>2</sub>-type structure, using *ab initio* calculations. The results confirm experimental findings that yttrium silicide nanowires are robust and conductive. In particular, the dependencies on nanowire thickness are analyzed. Furthermore, calculations show that the vacancy formation in stoichiometric nanowires is energetically favorable. The total energy of the nanowires is decomposed into the bulk, surface, and edge contributions. An equation is proposed for the cohesive energy  $E_c(n,m)$  of an arbitrary wire as a function of its cross-section dimensions  $n$  and  $m$ , which can be further reduced to the nearly linear relationship between the cohesive energy and composition. A comparison with recent epitaxial growth experiments is given.

DOI: [10.1103/PhysRevB.75.035406](https://doi.org/10.1103/PhysRevB.75.035406)

PACS number(s): 87.16.Ac, 81.05.Zx

## I. INTRODUCTION

Metal silicide nanowires (MSNWs) are of interest as potential building blocks for nanoelectronics since their morphology, size, and electronic properties make them suitable for fabricating low-resistance interconnects,<sup>1</sup> components for molecular electronics,<sup>2</sup> and nanoscale devices. Their practical synthesis through the epitaxial growth of a variety of self-assembled rare earth (RE) MSNW has been reported.<sup>3–10</sup> When a metal film is deposited on Si(001) surface and annealed, it forms compounds of nearly MSi<sub>1.7</sub> stoichiometry, hexagonal AIB<sub>2</sub>-type structure, with the  $c$  axis parallel to the surface. The self-assembled MSNW can be grown on Si if the magnitude of the lattice mismatch between the epilayer and substrate is large along one crystal axis and small along the perpendicular axis, leading to the formation of long, straight wires confined in their width due to the effects of strain. This was first observed for Dy (Refs. 3–7) and later for Er,<sup>3,8</sup> Ho,<sup>5,9</sup> Gd,<sup>10</sup> and (though not from RE metals) Sc (Ref. 3) and Y.<sup>1,11</sup> These wires have the widths and heights in the range of 1.5–11 and 0.2–4 nm, respectively, depending on the lattice mismatch. The average lengths of the nanowires were in the range 150–450 nm and are determined primarily by kinetic factors.<sup>1,3</sup> They exhibit atomically flat surfaces, are also robust, straight, and conductive, which are useful properties for any potential application in nanodevice architectures.<sup>1</sup>

Despite of the sustained experimental progress in the synthesis, characterization, and possible application of MSNW, there remains rather limited theoretical description yet. Issues of relative stability of small clusters and nanowires were theoretically considered for hexagonal<sup>12–14</sup> and pentagonal<sup>12,15</sup> smallest cross-section shapes. Previously we have explored metal-silicon structures from nanotube point of view,<sup>16</sup> demonstrating that the Si isomorphs of the thinnest fullerene tubes (2,2) and (3,0) can be stabilized by placing certain metal atoms along the tube axis. The structures obtained in the course of relaxation appeared, somewhat unexpectedly, to be identical to the bulk-derived metal silicide wires; we have explored their stability by computing and mapping the cohesive energies.<sup>16,17</sup> The results however

were limited to the thinnest wire of one primitive cell cross section, while experimentally observed MSNW are often several times thicker. It is important to extend the analysis to the larger cross sections, and to see if general regularities in cohesive energy ( $E_c$ ) behavior can be revealed. In this paper, we have used atomistic simulations to investigate the structure, energetics, electronic, and mechanical properties of such MSNW of various cross sections and accordingly of various stoichiometries. We concentrate our attention on yttrium silicide nanowires (YSNW). Although yttrium has no  $f$  electrons—a formal attribute of the rare earths—still it is generally associated with the RE elements due to its similar physical and chemical properties. Therefore the study of YSNWs can provide an idea of the properties of the whole group of RE silicide nanowires. It should be also pointed out that YSNWs have lattice mismatch close to zero with the Si(001) surface in the axial direction of the nanowire,<sup>1,3</sup> which makes in principle formation of long, high aspect ratio wires more likely.

The paper is structured as follows. In Sec. II we describe the computational methods. Section III shows that the approach correctly accounts (compared with other theoretical methods and sometimes also with experimental data) for the properties of bulk YSi<sub>2</sub> and also for the properties of the thinnest YSNWs. Section IV discusses the relative stability of several YSNWs with different cross-section dimensions and based on that a general equation for the prediction of the nanowire cohesive energy is proposed. Section V before the summary discusses the formation of vacancies in YSNWs and their influence on the electronic and structural properties of the possible wires.

## II. COMPUTATIONAL APPROACH

All calculations in this work are performed using density functional theory (DFT) (Refs. 18 and 19) and the plane wave method<sup>20,21</sup> implemented in the Quantum-ESPRESSO package.<sup>22</sup> For the treatment of the exchange and correlation term we use the local spin-density approximation (LSDA) within the generalized gradient approximation (GGA).<sup>23,24</sup> Calculations have been done using ultrasoft Vanderbilt

pseudopotentials.<sup>25</sup> For partial occupancies we used Methfessel-Paxton smearing method.<sup>26</sup> The width of the smearing was chosen 0.272 eV (0.02 Ry). The cutoff energy of 30 Ry for the plane wave expansion and 210 Ry for the electronic charge density was found to be sufficient to obtain convergent results. The  $\Gamma$  point was used for the Brillouin zone integrations in the case of the finite structures, and  $1 \times 1 \times 16$   $k$ -point sampling along the nanowire axis was used for the infinite nanowires. For the bulk and slab structures the  $k$ -point sampling was  $8 \times 8 \times 8$  and  $16 \times 1 \times 16$ , respectively. In all cases the Monkhorst-Pack scheme<sup>27</sup> was used. The total energy was converged to  $10^{-6}$  Ry and ionic positions were optimized until the forces acting on them were less than 0.026 eV/Å ( $10^{-3}$  Ry/Bohr). To study properties of finite clusters the supercell geometry was taken to be a tetragonal cell with lattice constant  $L$  sufficiently big to avoid interactions between finite clusters ( $\sim 1$  nm vacuum distance was chosen between structures). For infinitely long structures the supercell was also tetragonal with the dimension  $L \times L \times L_z$ , where the  $z$  direction is defined as the axial direction of the nanowire. Different cells with different  $L_z$  values were considered in order to obtain the optimized value for each studied nanowire. Similar optimization was performed in the case of two-dimensional and bulk systems.

### III. THINNEST YTTRIUM SILICIDE NANOWIRES

Low dimensional forms of materials may have properties quite different from those of their archetype bulk structures. Throughout this paper we illustrate this with few examples for our particular nanostructures. Bulk binary silicides of several RE metals and also Y exhibit the  $AlB_2$  structure and have been reported to have the approximate formula  $MSi_{1.7}$ .<sup>28</sup> Deviation from  $MSi_2$  suggests that vacancies exist in the silicon sublattice and indeed extensive studies<sup>28</sup> confirm that in a unit cell of nine sites, one of the six sites occupied by the Si atoms is vacant. Our computed structural parameters  $a$  and  $c/a$ , for the stoichiometric  $YSi_2$  structure, are 4.108 Å and 0.960, respectively, being in good agreement with other theoretical calculations.<sup>29</sup> The obtained values, however, are rather different from the experimental ones ( $a=3.842$  Å,  $c/a=1.077$ ).<sup>28,29</sup> This discrepancy is mainly due to the presence of silicon vacancies in epitaxial samples.<sup>29</sup> We have also calculated the bulk modulus  $B$  for  $YSi_2$  and the obtained value  $B=85$  GPa is rather small compared, for example, to the experimentally obtained  $B=169$  GPa for  $CoSi_2$ .<sup>30</sup>

Analysis of the wires, YSNW, we begin with the description of the properties of the thinnest possible freestanding YSNW of  $AlB_2$ -type structure, with diameters of the order of  $\sim 0.5$  nm. The MSNWs grown on Si(001) have typical height of about 0.5 nm,<sup>3</sup> so the discussion of very thin nanowires is justifiable. As pointed out in the Introduction, such nanowire can be viewed as a (2,2) silicon nanotube with an axially placed metallic chain of atoms, that is metal endohedral silicon nanotube, M@SiNT. Each metal is located in the center of a distorted hexagonal prism silicon cage [see, for example, Fig. 1(b)]. It is already known that pure (2,2) SiNT lacks stability.<sup>16,31</sup> Using *ab initio* calculations we have pre-

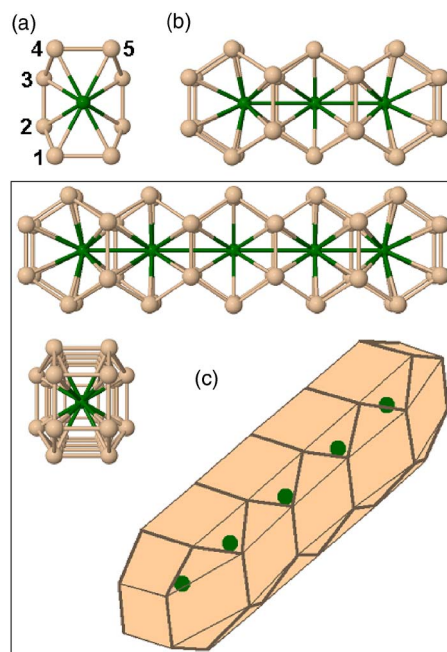


FIG. 1. (Color online) (a) Axial view of the thinnest infinite nanowire of  $AlB_2$ -type structure; beige (light gray) is for Si and green (dark gray) is for Y atoms. (b) Side view of the  $Y_3Si_{28}$  cluster. (c) Side view of the  $Y_5Si_{44}$  cluster (top), and its axial cap view (center); bottom axonometric projection clearly shows connection of the nanowires (here  $Y_5Si_{44}$  cluster) with the morphology of fullerene nanotube (2,2), by highlighting the hexagonal facets of the Si frame.

viously described<sup>16</sup> how the SiNT of chiral symmetry (2,2) is stabilized by the axially placed Sc and several other transition metal atoms. Similarly, in the present case the reinforcement by the internal Y-Si bonding stabilizes the SiNT and the resulting structure of stoichiometry  $YSi_8$  possesses large cohesive energy  $E_c=3.92$  eV. For comparison, the calculated bulk cohesive energy ( $E_{bc}$ ) for  $YSi_2$  is 4.98 eV. The optimized structure of the  $YSi_8$  nanowire is shown in Fig. 1(a). To calculate the structure we have used the smallest unit cell with eight silicon atoms and one yttrium atom. In that unit cell we can distinguish two groups of atoms lying in two parallel planes, normal to the wire axes. The distance between these planes is half of the nanowire lattice parameter  $a(YSi_8)=3.824$  Å. One in-plane atomic group consists of Y surrounded by four silicon atoms [see Fig. 1(a)], all at equal distances from Y,  $d_{Y-Si}=2.812$  Å. The second planar group includes only four silicon atoms, all at identical but larger distance from Y,  $d_{Y-Si}=2.962$  Å. In both cases the Y-Si distances are shorter than the corresponding values in the bulk,  $d_{Y-Si}(YSi_2)=3.085$  Å. The Si-Si bond lengths are  $d_{12}=2.401$  Å,  $d_{23}=2.372$  Å,  $d_{34}=2.401$  Å, and  $d_{45}=2.593$  Å, where the subindexes correspond to atomic labels in Fig. 1(a). All these values are equal or bigger than the  $d_{Si-Si}=2.372$  Å in bulk  $YSi_2$ .

To assess the mechanical rigidity of the YSNWs we have calculated the Young's modulus, which accounts for the response to axial stress. We found that the nanowire is quite stiff, with the Young's modulus of  $Y=144$  GPa (assuming cross-section area as  $44$  Å<sup>2</sup>, to include the Si radii). The

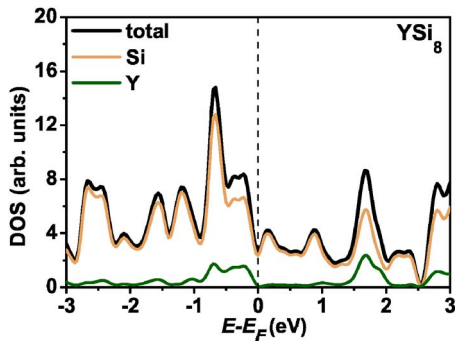


FIG. 2. (Color online) The density of states of the thinnest  $\text{YSi}_8$  nanowire. The beige (light gray) and green (dark gray) lines are the projection of the total DOS (thicker black line) on the Si and Y sublattices, respectively.

tension was estimated to be  $1.2 \text{ eV}/\text{\AA}$  for 2% strain. Similar results were reported<sup>16</sup> for the (3,0)  $\text{Zr@SiNT}$ , what may suggest that the type of the metal has marginal influence on the nanowire stiffness. This value is in a ballpark agreement with the mentioned above bulk modulus  $B=85 \text{ GPa}$ , as their relationship  $Y=3(1-2\nu)B$  holds well at the Poisson ratio  $\nu \approx 0.2$ , a typical value for solids.

Turning now to electronic properties, we found that the infinite nanowire is metallic with substantial density of electronic states (DOS) at the Fermi level. Figure 2 presents DOS of YSNW and also the projection of the total DOS on the metal chain and the silicon-only frame. Interestingly, the contribution of yttrium atoms to the DOS is very small at the Fermi level ( $E_F$ ). This result marks the difference between the bulk  $\text{YSi}_2$  and the YSNW, since both theoretical<sup>32,33</sup> and experimental<sup>34</sup> studies confirm that the Y  $d$ -state contribution to the DOS of  $\text{YSi}_2$  is significant at  $E_F$  and together with the Si contribution is responsible for its metallic character. Going back to Fig. 2, the nonzero value for DOS at  $E_F$  is mainly due to the contribution from the silicon frame, what may explain the metallic character of all RE silicide nanowires obtained experimentally.<sup>1</sup>

To ensure that stability is retained at finite length as well, we considered finite clusters  $\text{Y}_3\text{Si}_{28}$  and  $\text{Y}_5\text{Si}_{44}$ , which were found to be also stable with cohesive energies equal to 3.80 and 3.85 eV, respectively. Figures 1(b) and 1(c) (top) show the lateral views of  $\text{Y}_3\text{Si}_{28}$  and  $\text{Y}_5\text{Si}_{44}$  clusters, respectively. The end atoms of the clusters reconstruct into square caps as can be clearly seen from the axial view in Fig. 1(c) (center). The  $\text{Y}_3\text{Si}_{28}$  and  $\text{Y}_5\text{Si}_{44}$  clusters have the highest occupied molecular orbital (HOMO) to the lowest unoccupied molecular orbital (LUMO) gaps of 164 and 59 meV, respectively.

Due to nonzero magnetic moment of Y, we have verified for possible magnetism of the YSNW by carrying out spin polarized calculations for all structures, and the optimized infinite and finite structures were found to be nonmagnetic. The magnetic moment of yttrium  $d$  electrons is quenched by the  $p(\text{Si})$ - $d(\text{Y})$  hybridization and as a result both finite and infinite nanowires are nonmagnetic.

#### IV. ENERGY DECOMPOSITION FOR THICKER WIRES

Let us now consider the MSNW with larger cross-sections, which can be viewed as  $n \times m$  repetition of the

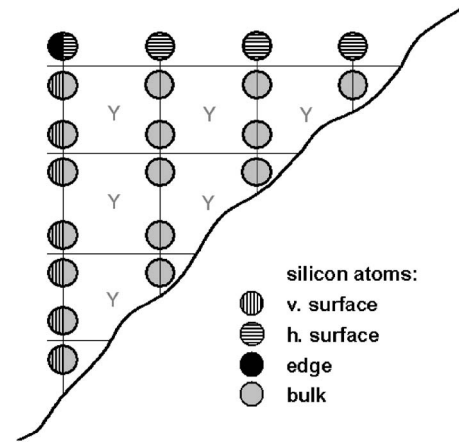


FIG. 3. Schematics shows the corner of the nanowire, distinguishing the bulk (gray) and extra surface (circles filled with horizontal and vertical lines), and edge (black) atoms. The bulk unit cell is formed by one Y and two Si atoms. For those unit cells which are adjacent to the surface there is an additional Si atom at the surface per unit cell. At the corner, an extra half of the Si atom shown in the figure is “shared” by two surfaces and should be counted as additional half-atom per edge.

primitive cell, properly terminated by extra Si atoms at the surfaces. Such wires can also be viewed as a bundle of the smaller, thinnest (discussed in Sec. III above) where every two neighboring nanowires share the silicon atoms, while the yttrium chains all lie parallel to the wire axis. We will call the arrangement of building blocks in the  $n$  and  $m$  directions as “vertical” and “horizontal,” respectively. In the special case of infinite  $n$  ( $m$ ) we get a vertical (horizontal) slab of thickness  $m$  ( $n$ ). For simplicity we consider here only wires with rectangular cross sections, but the study can be extended to any desired cross section. The  $n \times m$  wire has a  $\text{Y}_{n \cdot m} \text{Si}_{2n \cdot m + 2n + 2m + 2}$  or  $\text{YSi}_{2(1+1/n+1/m+1/n \cdot m)}$  stoichiometry, where one can distinguish  $3n \cdot m$  bulk atoms from the extra  $2n + 2m$  surface atoms and two edge atoms. In Fig. 3 we have shown schematics of the nanowire atoms assignment to the bulk, surface, and the edge. Both surfaces and all edges obviously contain extra Si atoms: the vertical surfaces add  $2n$ , the horizontal add  $2m$ , and each edge adds  $1/2$  of an atom. The bulk atoms include  $2n \cdot m$  silicon atoms and  $n \cdot m$  yttrium atoms. The composition can be characterized by the fraction of metallic atoms,  $x \equiv n \cdot m / (3n \cdot m + 2n + 2m + 2) = 1 / (3 + 2/n + 2/m + 2/n \cdot m)$ , so that for the thinnest  $1 \times 1$  wire  $x = 1/9$  and for the  $\text{inf} \times \text{inf}$  bulk  $x = 1/2$ . In Figs. 4(a)–4(c) we have shown three computed (fully relaxed) examples of the rectangular section wires with dimensions  $1 \times 5$ ,  $3 \times 1$ , and  $3 \times 3$ , respectively.

Direct energy computation of larger wires becomes exceedingly expensive as the number of atoms in a computational supercell increases rapidly as  $\sim n \cdot m$ . To circumvent this difficulty, energy decomposition approach<sup>35</sup> suggests separating the contributions that scale differently with the thickness  $d$ : that is from the bulk ( $\sim d^2$ ), surface ( $\sim d^1$ ) and the edges (constant  $\sim d^0$ ). With this in mind, the total energy of  $\text{Y}_{n \cdot m} \text{Si}_{2n \cdot m + 2n + 2m + 2}$  wire can be represented by the formula

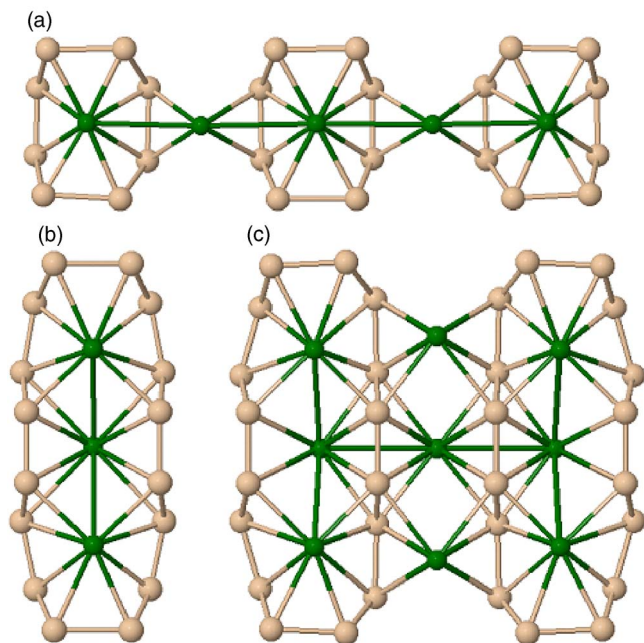


FIG. 4. (Color online) Axial view of fully relaxed nanowires with three different cross sections: (a) “horizontal”  $1 \times 5$ , (b) “vertical”  $3 \times 1$ , and (c)  $3 \times 3$  dimensions.

$$E_t(n, m) = -N_t E_{bc} + 2n\gamma_1 + 2m\gamma_2 + 4\varepsilon + N_Y E_Y + N_{Si} E_{Si}, \quad (1)$$

where  $E_{bc}$  is the bulk cohesive energy,  $\gamma_1$  and  $\gamma_2$  are the vertical and horizontal surface energies per unit cell (or atom, in this case),  $\varepsilon$  is the edge energy,  $E_Y$  and  $E_{Si}$  are the metal and silicon atomic energies,  $N_Y = n \cdot m$  and  $N_{Si} = 2n \cdot m + 2n + 2m + 2$  are the numbers of metal and silicon atoms, so that  $N_t = N_Y + N_{Si}$  is the total number of atoms. Equation (1) is common for macroscopic systems (where  $\varepsilon$  can be neglected), and even used for the surface energy definition. However, extrapolating its utility into the nanoscale cannot be taken for granted due to the close proximity and possible mutual effects between the surfaces, edges, and the bulk. One must verify if actual directly computed energies for the very small structures follow Eq. (1) closely. In other words, the question is if the energy parameters, i.e., coefficients in Eq. (1) retain approximately invariant, universal values among the variety of wires, for any  $n, m$  pairs. Formally, the values for the four parameters  $E_{bc}$ ,  $\gamma_1$ ,  $\gamma_2$ , and  $\varepsilon$ , can be easily obtained by calculating the total energies of four different wires (that is four different sets of  $n, m$ ) but it is not obvious that one can use then these values to calculate  $E_t(n, m)$  of any other desired nanowire. While describing now how to find such parameters, we will also try to answer the question how accurate Eq. (1) can be. For this purpose let us define the system cohesive energy per atom

$$E_c(n, m) = [N_Y E_Y + N_{Si} E_{Si} - E_t(n, m)] / N_t, \quad (2)$$

where  $E_t(n, m)$  is given by Eq. (1). Clearly, for very large  $n, m$  this approaches the bulk value,  $E_c(inf, inf) = E_{bc}$ . Using Eqs. (1) and (2) one can define now the total nanowire sur-

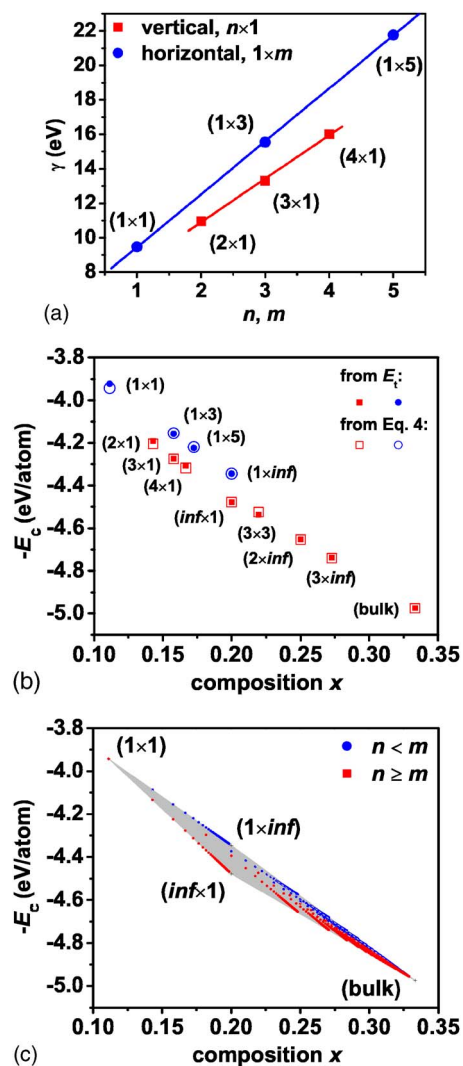


FIG. 5. (Color online) (a) Total surface energy  $\gamma$  described by Eq. (3) versus the nanowire dimensions  $n$  (vertical, squares) and  $m$  (horizontal, circles). (b) Cohesive energy  $E_c$  per atom as a function of composition  $xN_Y/N_t$ . The open and filled symbols correspond to the values obtained from simple Eq. (4) and by directly computing  $E_t$  in the Eq. (2), respectively. (c)  $E_c$  calculated using Eq. (4) for a broad range of nanowires with  $n$  and  $m$  values (here, 1 to 100). Notably, all the values are confined within a cigar-shaped area (light gray) of a maximum width  $0.4(\gamma_1 - \gamma_2)$ , which for  $\gamma_1 = \gamma_2 = 2\varepsilon$  becomes an exact linear relationship. Here  $\gamma_1 = 1.243$ ,  $\gamma_2 = 1.576$ , and  $\varepsilon = 0.914$  eV.

face energy as a difference between the bulk and wire cohesive energies per atom, multiplied by  $N_t$

$$\gamma(n, m) = N_t [E_{bc} - E_c(n, m)] = 2n\gamma_1 + 2m\gamma_2 + 4\varepsilon. \quad (3)$$

Based on the values of  $E_Y$ ,  $E_{Si}$ ,  $E_{bc}$ , and  $E_t(n, m)$  directly obtained from computations, we now plot in Fig. 5(a) the total surface energy given by Eq. (3) as a function of the number  $n$  of vertical or the number  $m$  of nanowires' horizontal size. (We used for  $E_{bc}$  the value obtained from calculations for the bulk  $YSi_2$  structure.) As can be seen from the figure, in both cases the computed values of  $\gamma(n, m)$  clearly

follow linear relationships, thus confirming Eq. (3). This result is important since we can define the same vertical surface energy for each wire from the family of  $n \times 1$  nanowires. The same is true for the horizontal surface energy for the nanowires fused in the horizontal direction ( $1 \times m$  family). From the slope of the straight lines we can obtain the values for  $\gamma_1$  and  $\gamma_2$ . Numerically, best linear fitting to the data of Fig. 5(a) yields the values  $\gamma_1=1.259$  and  $\gamma_2=1.537$  eV. Surface energies can be also obtained independently from more accurate calculations for slab or other confined systems.<sup>36</sup> The corresponding surface energies for the thinnest slabs in both directions are 1.243 and 1.576 eV for  $\gamma_1$  and  $\gamma_2$ , respectively. The agreement with the values above is remarkably good (the difference is 1.3% and 2.5% for  $\gamma_1$  and  $\gamma_2$ , respectively) especially if one takes into account the fact that only few data points [see Fig. 5(a)] were used to calculate the slopes.

It is well known that for the thin slabs  $\gamma_1$  and  $\gamma_2$  may vary with the slab thickness.<sup>37</sup> It was also demonstrated that the value for  $E_{bc}$  calculated from the bulk structure may lead to errors in surface energies.<sup>37</sup> Since our goal in this work is to explore the existence of universal parameters, which are useful to predict the  $E_c$  of nanowires, we estimate the values for  $\gamma_1$  and  $\gamma_2$  rather than calculate them to extreme accuracy. The vertical slab consists of a set of graphenelike vertical sheets of  $sp^2$  bonded silicon atoms separated by yttrium layers. In this arrangement the silicon monolayers should not too strongly interact with each other, and as a consequence  $\gamma_1$  does not depend significantly on the thickness of the slab even for small  $m$ . This is not the case of horizontal slabs, in which the silicon atoms do not form bonds in the planes parallel to the slab surfaces but are rather arranged in planes perpendicular to them and, consequently, stronger dependence on slab thickness  $n$  can be expected. Indeed, for the slab with thickness  $n=2$ ,  $\gamma_2$  was calculated to be 1.291 eV (for  $n=1$ ,  $\gamma_2=1.576$  eV), however, further increase of slab thickness does not change  $\gamma_2$  significantly since for  $n=3$ ,  $\gamma_2=1.305$  eV.

Summarizing the results, we can accept the value for  $\gamma_1$  similar for all nanowires and equal to 1.243 eV. The horizontal surface energy decreases from  $\gamma_2=1.576$  eV, for the nanowire family  $1 \times m$ , to the value of 1.291 eV, for nanowires with  $n>1$ . The value of  $\varepsilon$  in Eq. (3) was calculated (fitted to data) to be 0.809 eV and is the same for all nanowires except those from the  $1 \times m$  family for which  $\varepsilon=0.914$  eV. (It is important to note that one cannot confirm the value of  $\varepsilon$  from independent calculations.)

The values for surface, edge, and bulk energies can be used now to calculate the cohesive energy  $E_c$  for any  $n \times m$  wires. Indeed, reversing Eq. (3) one can find  $E_c$  (per atom) as

$$E_c(n,m) = E_{bc} - (2n\gamma_1 + 2m\gamma_2 + 4\varepsilon)/N_t. \quad (4)$$

Figure 5(b) depicts  $E_c(n,m)$  as a function of composition  $x = N_Y/N_t = 1/(3+1/n+1/m+1/n \cdot m)$  for all nanowires. The open symbols correspond to the values predicted by Eq. (4) and the filled symbols mark the values obtained from the computed total energies, following Eq. (2). As can be seen from the figure, Eq. (4) gives very accurate predictions. In all cases the error does not exceed 20 meV. More precise cal-

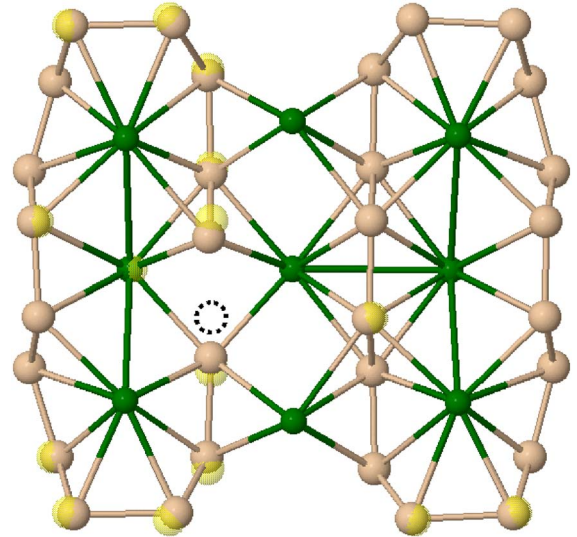


FIG. 6. (Color online) Relaxed structure of  $Y_{18}Si_{63}$  (only half of the unit cell is shown). The vacancy site is marked by a black dotted circle. Yellow translucent (light gray) balls indicate the initial positions of atoms of the complete  $Y_{18}Si_{64}$  nanowire, to show the degree of relaxation around the vacancy.

culations of surface energies can further improve the accuracy of Eq. (4), which is especially important for larger nanowires, when the cohesive energies are very close.

## V. SILICON DEFICIENT NANOWIRES

Although ideal thin wire structure clearly shows an excess of silicon due to surface closure ( $x < 0.33$ ), the nanowires produced experimentally are nonstoichiometric, often near  $YSi_{1.7}$  with  $x=0.37$ , as was mentioned in the Introduction. This suggests that silicon vacancies exist not only in the bulk structures, but also in one-dimensional systems. To explore the properties of silicon deficient nanowires we created vacancies in the  $3 \times 3$  ( $Y_9Si_{32}$ ) nanowire shown in Fig. 4(c). To ensure that the distance between the vacancies is similar to the observed experimentally we considered a unit cell two times bigger than that shown in Fig. 4(c), corresponding to a structure with stoichiometry  $Y_{18}Si_{64}$ . The vacancy was created by removing one of the Si atoms closest to the wire axis. This corresponds to a vacancy concentration  $z=1/82$  (1.2%). The resulting relaxed structure  $Y_{18}Si_{63}$  is shown in Fig. 6. To evaluate the relative stability of  $Y_{18}Si_{63}$  and  $Y_{18}Si_{64}$ , we have first calculated the vacancy formation energy  $E_{vac}$  given by the expression

$$\begin{aligned} E_{vac} &= E_t(Y_{18}Si_{63}) + E_{bSi} - E_t(Y_{18}Si_{64}) \\ &= 82E_c(Y_{18}Si_{64}) + \mu_{Si} - 81E_c(Y_{18}Si_{63}), \end{aligned} \quad (5)$$

where  $E_t(\cdot)$  and  $E_c(\cdot)$  are the total and cohesive energies, respectively, of  $Y_{18}Si_{63}$  and  $Y_{18}Si_{64}$  nanowires, and  $E_{bSi}$  and  $\mu_{Si}$  are the silicon bulk energy and—in general case—in its chemical potential. The calculated values for  $E_c(Y_{18}Si_{63})$  and  $E_c(Y_{18}Si_{64})$  are 4.542 and 4.536 eV/atom, respectively. The value of  $\mu_{Si}=-4.485$  eV was overestimated in our calcula-

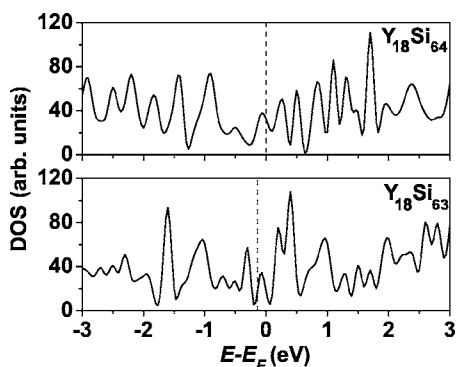


FIG. 7. DOS of the  $Y_{18}Si_{64}$  (top) and  $Y_{18}Si_{63}$  (bottom) nano-wires. Note that  $E=0$  for both plots is chosen at the  $E_F$  for perfect  $Y_{18}Si_{64}$  wire, whereas  $E_F$  for Si-depleted  $Y_{18}Si_{63}$  is lowered by 0.14 eV.

tions if compared with experimental data.<sup>38</sup> From Eq. (5) we obtained that  $E_{vac}=-0.435$  eV has a small but negative value, meaning that the vacancy formation is favorable. This is an important indication that not only in bulk metal silicides<sup>28</sup> but similarly in YSNW the strain induced by the large size difference between Si and the metal is relaxed by formation of Si vacancies. Furthermore, we have checked that if one more Si atom is removed to form the  $Y_9Si_{31}$  structure, and the separation between the vacancies becomes two times smaller than in  $Y_{18}Si_{63}$ , the formation energy becomes positive ( $E_{vac}=0.303$  eV). This suggests the existence of an optimum for the fraction of Si vacant sites formation, as observed experimentally.<sup>28</sup>

$Y_{18}Si_{64}$  without vacancies has a lattice parameter  $a(Y_{18}Si_{64})=7.666$  Å. Interestingly, in presence of vacancies in the nanowire the lattice parameter does not vary too much since  $a(Y_{18}Si_{63})=7.657$  Å. The lattice parameter of  $Y_9Si_{32}$ ,  $a(Y_9Si_{32})=a(Y_{18}Si_{64})/2=3.833$  Å, is also close to that for  $YSi_8$  nanowire, so we can conclude that there is no significant variation of the lattice parameter with nanowire diameter.

The effect of vacancies on the DOS is shown in Fig. 7 (bottom) and for comparison is also shown the DOS for the  $Y_{18}Si_{64}$  structure, see Fig. 7 (top). The Fermi levels for  $Y_{18}Si_{63}$  and  $Y_{18}Si_{64}$  are 1.75 and 1.89 eV, respectively, so due to the presence of vacancies there is a small shift of the  $E_F$ , by 0.14 eV towards lower energies. Using *ab initio* calculations Magaud *et al.*<sup>33</sup> obtained for bulk  $YSi_{1.7}$  and the vacancy concentration of 11.1% a 1.5 eV shift of the  $E_F$  toward lower energies. In our case the shift of the Fermi energy is approximately ten times smaller which is understandable if one takes into account that the considered vacancy concentration is also ten times smaller. From Fig. 7 we can see also that the DOS at  $E_F$  is nearly twice less in  $Y_{18}Si_{63}$  than in  $Y_{18}Si_{64}$ , which again points towards better stability<sup>33</sup> of this structure relative to the stoichiometric nanowire.

To compare the stability of  $Y_{18}Si_{63}$ ,  $Y_{18}Si_{64}$ , and bulk  $YSi_2$  we calculated for each structure the zero-temperature limit of the Gibbs free energy of formation per atom,  $\delta G$ , defined as

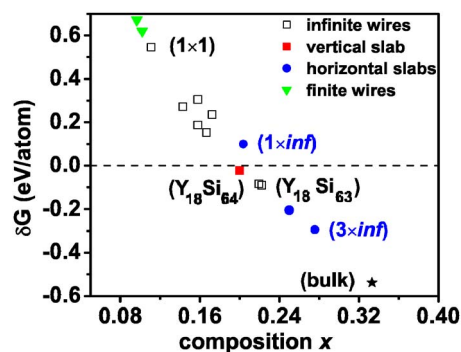


FIG. 8. (Color online) Gibbs free energy of formation per atom,  $\delta G$ , as a function of composition  $x=N_Y/N_t$  [see Eq. (6)]. All structures with positive  $\delta G$  are metastable and the least stable from that group are the short wires (clusters). At the boundary (dashed line) of thermodynamic stability appears the thinnest vertical slab with  $\delta G=-0.022$  eV. The points for  $Y_{18}Si_{63}$  and  $Y_{18}Si_{64}$  wires overlap since both structures are very close in energy.

$$\delta G = -E_c - x\mu_Y - (1-x)\mu_{Si}, \quad (6)$$

where  $E_c$  is the cohesive energy of some  $Y_xSi_{1-x}$ ,  $x=N_Y/N_t$  [i.e.,  $1/(3+1/n+1/m+1/n\cdot m)$  for our wires] is the composition, and  $\mu_Y$  and  $\mu_{Si}$  are the chemical potentials of Y and Si, respectively. (Here again the obtained value for  $\mu_Y=-4.34$  eV is overestimated if compared with experimental data.<sup>38</sup>) The results of our calculations for  $\delta G$  are summarized in Fig. 8. From the figure one can see that both  $Y_{18}Si_{63}$  and  $Y_{18}Si_{64}$  are thermodynamically stable (at list at  $T=0$  K), since  $\delta G(Y_{18}Si_{63})=-0.089$  eV and  $\delta G(Y_{18}Si_{64})=-0.083$  eV have negative values, but are of course less stable than the bulk structure with  $\delta G(YSi_2)=-0.538$  eV. As expected from our previous analyses,  $Y_{18}Si_{63}$  is slightly more stable than  $Y_{18}Si_{64}$  and the difference between  $\delta G(Y_{18}Si_{63})$  and  $\delta G(Y_{18}Si_{64})$  multiplied by 82 (total number of atoms in the unit cell) gives us approximately the value for the vacancy formation energy obtained before. From Fig. 8 one can also see that the thinnest nanowires are energetically less favorable; in the experiments however very thin (with small heights) wires can be formed<sup>1</sup> since they are stabilized by the contact with silicon substrate.

## VI. SUMMARY

In summary, we have studied the structures, stability, and electronic properties of yttrium silicide nanowires. Especially we have extended the approach towards larger (thicker) wires where direct computations become costly due to increasing number of atoms in the cross section. To overcome this difficulty and also to obtain additional insight, we have used energy decomposition approach,<sup>35</sup> where the total energy is separated into contributions from the bulk, surfaces, and the edges between the facets. Such separation, although not rigorous at the nanoscale, since possible strong interactions between the surfaces and with the edges can break their individual meaning, holds nevertheless very well. Universal (that is almost invariant in going from wire to wire) energy parameters were determined from several ba-

sic computed structures, and based on their values an equation was obtained for the cohesive energy of arbitrary nanowires. We obtained that the energy of nanowire surface perpendicular to the growth direction is higher than that of the surface parallel to that direction. We obtained also that the nanowires with small cross-sections are energetically less favorable. The metallic character of the metal-silicide nanowires is confirmed and found to be associated with the electronic properties of the silicon frame rather than to the metal chain. We also found that the formation of silicon vacancies is energetically favorable when the distance between them is of the order of double the axial lattice parameter of the wire; however when the vacancies are too many and too close to each other (at lattice parameter distance) the formation en-

ergy becomes positive. Our energy decomposition analysis can be extended to nanowires with nonrectangular cross-sections and can be also used to predict the stability of non-wire systems such as, for example, zero-dimensional quantum dots. (In the latter case, in addition to the  $\sim d^3$ , facets  $\sim d^2$ , and edges  $\sim d^1$  energies, a contribution from the vertices  $\sim d^0$  must not be omitted.)

#### ACKNOWLEDGMENTS

We acknowledge support by the Robert A. Welch Foundation and the Air Force Research Laboratory, Materials Directorate. We thank David J. Srolovitz for stimulating discussion.

\*Corresponding author. Electronic address: biy@rice.edu

<sup>1</sup>B. Z. Liu and J. Nogami, *Nanotechnology* **14**, 873 (2003).

<sup>2</sup>J. R. Heath, P. J. Kuekes, G. S. Snider, and R. S. Williams, *Science* **280**, 1716 (1998).

<sup>3</sup>Y. Chen, D. A. A. Ohlberg, and R. S. Williams, *J. Appl. Phys.* **91**, 3213 (2002).

<sup>4</sup>B. Z. Liu and J. Nogami, *J. Appl. Phys.* **93**, 593 (2003).

<sup>5</sup>J. Nogami, B. Z. Liu, M. V. Katkov, C. Ohbuchi, and N. O. Birge, *Phys. Rev. B* **63**, 233305 (2001).

<sup>6</sup>C. Preinesberger, S. Vandr e, T. Kalka, and M. D ahne-Prietsch, *J. Phys. D* **31**, L43 (1998).

<sup>7</sup>C. Preinesberger, S. K. Becker, S. Vandr e, T. Kalka, and M. D ahne, *J. Appl. Phys.* **91**, 1695 (2002).

<sup>8</sup>Y. Chen, D. A. A. Ohlberg, G. Medeiros-Ribeiro, Y. A. Chang, and R. S. Williams, *Appl. Phys. Lett.* **76**, 4004 (2000).

<sup>9</sup>C. Ohbuchi and J. Nogami, *Phys. Rev. B* **66**, 165323 (2002).

<sup>10</sup>D. Lee and S. Kim, *Appl. Phys. Lett.* **82**, 2619 (2003).

<sup>11</sup>M. Katkov and J. Nogami, *Bull. Am. Phys. Soc.* **47**, 283 (2002).

<sup>12</sup>A. N. Andriotis, G. Mpourmpakis, G. E. Froudakis, and M. Menon, *New J. Phys.* **4**, 78 (2002).

<sup>13</sup>A. K. Singh, T. M. Briere, V. Kumar, and Y. Kawazoe, *Phys. Rev. Lett.* **91**, 146802 (2003).

<sup>14</sup>A. K. Singh, V. Kumar, and Y. Kawazoe, *J. Mater. Chem.* **14**, 555 (2004).

<sup>15</sup>M. Menon, A. N. Andriotis, and G. E. Froudakis, *Nano Lett.* **2**, 301 (2002).

<sup>16</sup>T. Dumitric a, M. Hua, and B. I. Yakobson, *Phys. Rev. B* **70**, 241303(R) (2004).

<sup>17</sup>T. Dumitrica, V. Barone, M. Hua, and B. I. Yakobson, in *Carbon Nanotubes*, edited by V. N. Popov and P. Lambin (Springer, Netherlands, 2006), p. 243.

<sup>18</sup>P. Hohenberg and W. Kohn, *Phys. Rev.* **136**, B864 (1964).

<sup>19</sup>W. Kohn and L. J. Sham, *Phys. Rev.* **140**, A1133 (1965).

<sup>20</sup>G. Kresse and J. Furthm uller, *Phys. Rev. B* **54**, 11169 (1996).

<sup>21</sup>G. Kresse and J. Furthm uller, *Comput. Mater. Sci.* **6**, 15 (1996).

<sup>22</sup>S. Baroni, A. Dal Corso, S. de Gironcoli, P. Giannozzi, C. Cavazzoni, G. Ballabio, S. Scandolo, G. Chiarotti, P. Focher, A. Pasquarello, K. Laasonen, A. Trave, R. Car, N. Marzari, and A. Kokalj, <http://www.pwscf.org/> (2006).

<sup>23</sup>J. P. Perdew, J. A. Chevary, S. H. Vosko, K. A. Jackson, M. R. Pederson, D. J. Singh, and C. Fiolhais, *Phys. Rev. B* **46**, 6671 (1992).

<sup>24</sup>J. P. Perdew, K. Burke, and M. Ernzerhof, *Phys. Rev. Lett.* **77**, 3865 (1996).

<sup>25</sup>D. Vanderbilt, *Phys. Rev. B* **41**, R7892 (1990).

<sup>26</sup>M. Methfessel and A. T. Paxton, *Phys. Rev. B* **40**, 3616 (1989).

<sup>27</sup>H. J. Monkhorst and J. D. Pack, *Phys. Rev. B* **13**, 5188 (1976).

<sup>28</sup>C.-X. Ji, M. Huang, J.-H. Yang, Y. A. Chang, R. Ragan, Y. Chen, D. A. A. Ohlberg, and R. S. Williams, *Appl. Phys. A: Mater. Sci. Process.* **78**, 287 (2004).

<sup>29</sup>L. Magaud, A. Pasturel, G. Kresse, and J. Hafner, *Phys. Rev. B* **55**, 13479 (1997).

<sup>30</sup>G. Gu enin, M. Ign et, and O. Thomas, *J. Appl. Phys.* **68**, 6515 (1990).

<sup>31</sup>E. Durgun, S. Tongay, and S. Ciraci, *Phys. Rev. B* **72**, 075420 (2005).

<sup>32</sup>L. Magaud, J. Y. Veuillen, D. Lollman, T. A. Nguyen Tan, D. A. Papaconstantopoulos, and M. J. Mehl, *Phys. Rev. B* **46**, 1299 (1992).

<sup>33</sup>L. Magaud, J. P. Julien, and F. Cyrot-Lackmann, *J. Phys.: Condens. Matter* **4**, 5399 (1992).

<sup>34</sup>L. Braicovich, E. Puppini, I. Lindau, A. Iandelli, G. L. Olcese, and A. Palenzona, *Phys. Rev. B* **41**, 3123 (1990).

<sup>35</sup>Y. Zhao and B. I. Yakobson, *Phys. Rev. Lett.* **91**, 035501 (2003).

<sup>36</sup>K. Rapcewicz, B. Chen, B. Yakobson, and J. Bernholc, *Phys. Rev. B* **57**, 7281 (1998).

<sup>37</sup>V. Fiorentini and M. Methfessel, *J. Phys.: Condens. Matter* **8**, 5526 (1996).

<sup>38</sup>C. Kittel, *Introduction to Solid State Physics* (Wiley, New York, 1996).